Electronic Supplementary Material (ESI) for Journal of Materials Chemistry A.

Electronic Supplementary Information (ESI)

High-performance solid-state hybrid supercapacitor enabled by metal-organic framework-derived multi-component hybrid electrodes of Co-N-C nanofibers and $Co_{2-x}Fe_xP$-N-C micropillars

Thangjam Ibomcha Singh,[a,b] G. Rajeshkhanna,[c] Tolendra Kshetri,[a] Nam Hoon Kim,*[a] Joong Hee Lee*[a,d]

[a]Department of Nano Convergence Engineering, Jeonbuk National University, Jeonju, Jeonbuk, 54896, Republic of Korea.

[b]Faculty of Science, Engineering & Technology, Swinburne University of Technology, PO Box 218, Hawthorn, VIC 3122, Australia.

[c]Department of Chemistry, National Institute of Technology, Warangal, India.

[d]Center for Carbon Composite Materials, Department of Polymer-Nano Science and Technology, Jeonbuk National University, Jeonju, Jeonbuk, 54896, Republic of Korea.

**Corrresponding author:* jhl@jbnu.ac.kr ; nhk@jbnu.ac.kr

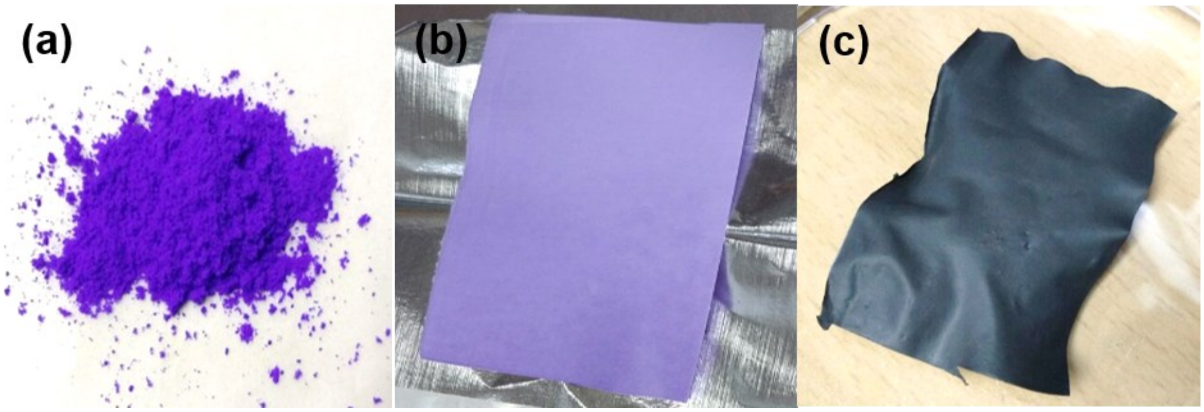

Fig. S1. Digital photographs of (a) ZIF-67, (b) electrospun PAN-ZIF-67 nanofiber mat before carbonization (EPZ-67-NFs), (c) electrospun PAN-ZIF-67 nanofiber mat after carbonization (Co-N-CNFs).

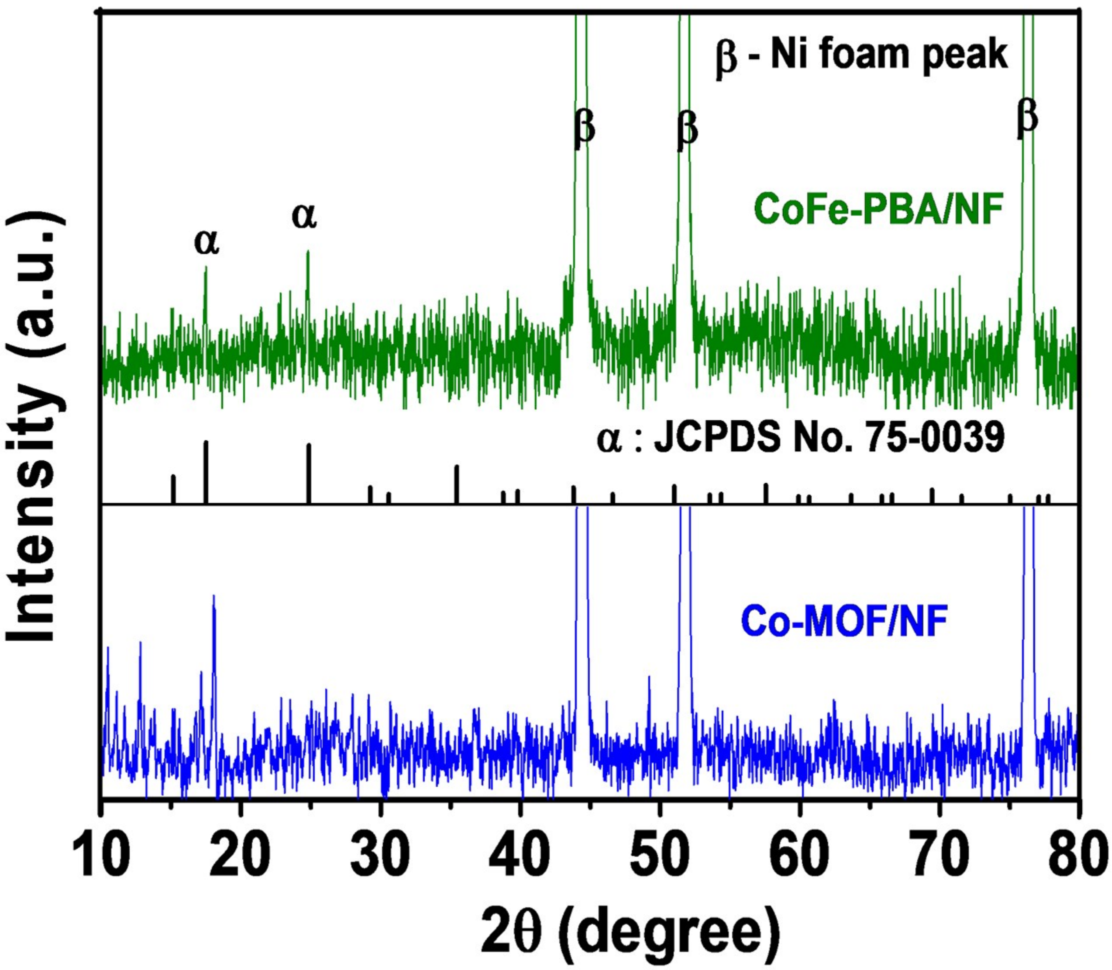

Fig. S2. PXRD patterns of Co-MOF/NF and CoFe-PBA/NF.

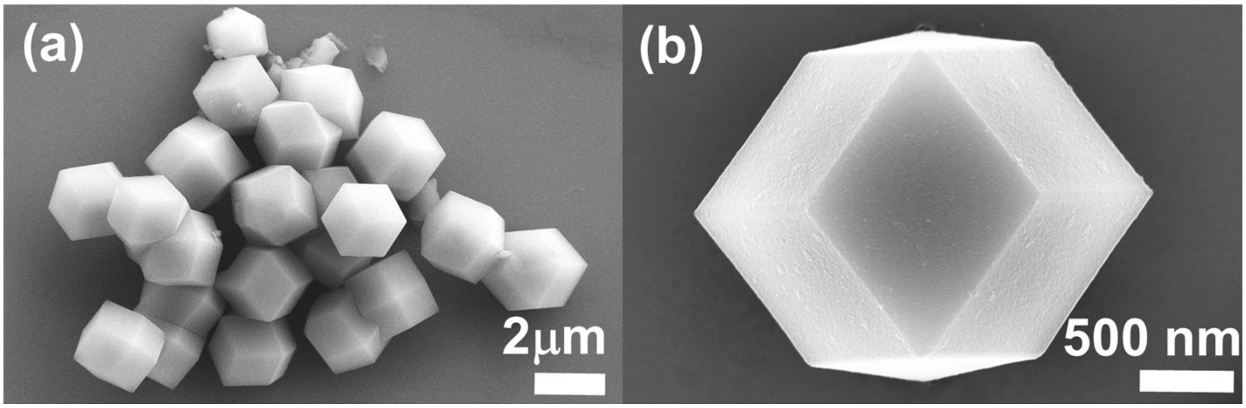

Fig. S3. (a and b) Low-and high-magnification FE-SEM images of ZIF-67.

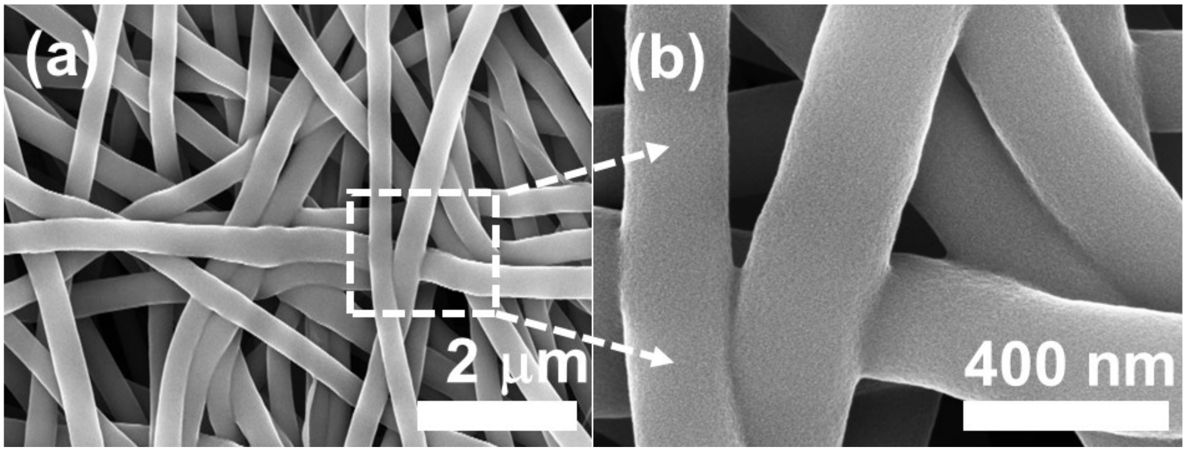

Fig. S4. (a and b) Low- and high-magnification FE-SEM images of electrospun PAN nanofibers (EP-NFs).

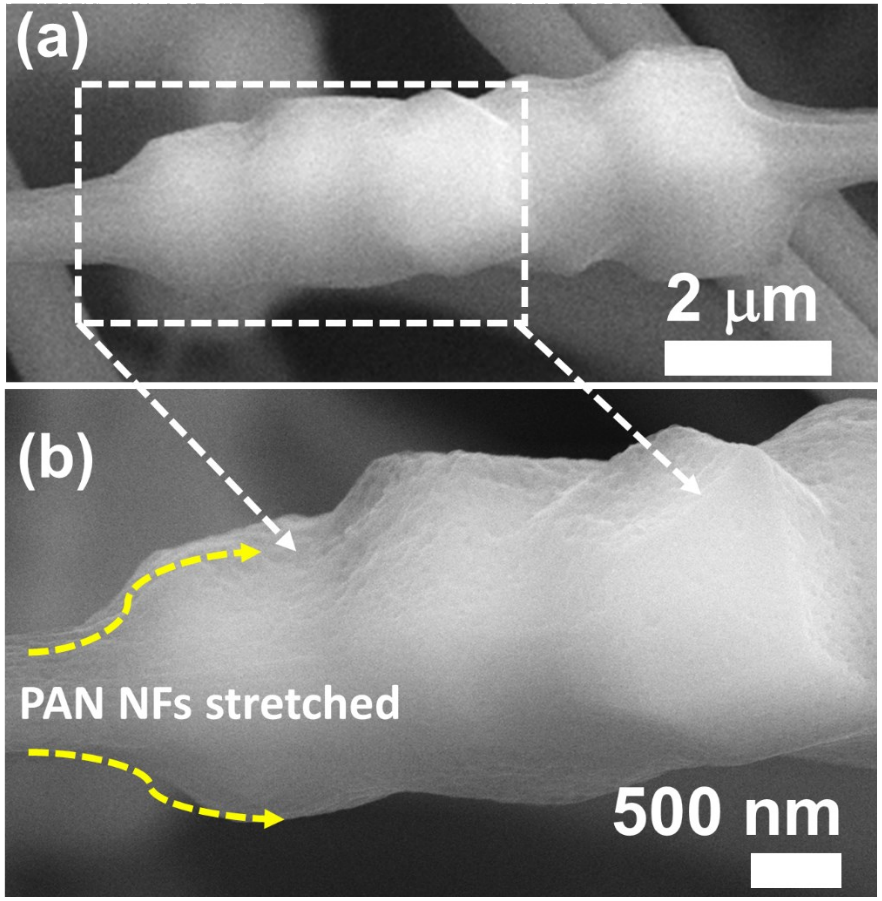

Fig. S5. (a and b) Low- and high-magnification FE-SEM images of electrospun PAN-ZIF-67 nanofibers (EPZ-67-NFs) before carbonization showing inclusion of ZIF-67 particles in PAN nanofibers.

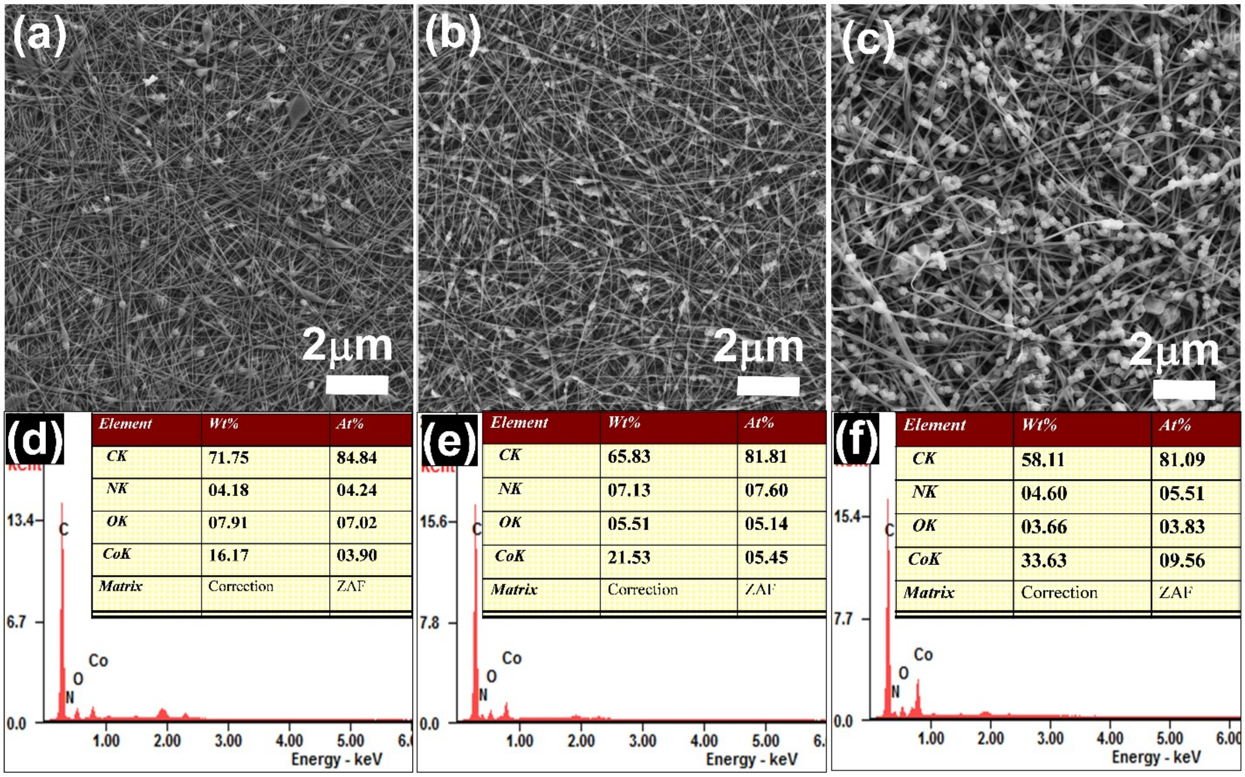

Fig. S6. FE-SEM images and corresponding EDS spectra of Co-N-CNFs prepared with PAN and ZIF-67, ZIF-67 to PAN weight ratios used (a and d) 1:10, (b and e) 1:5 and (c and f) 1:3.

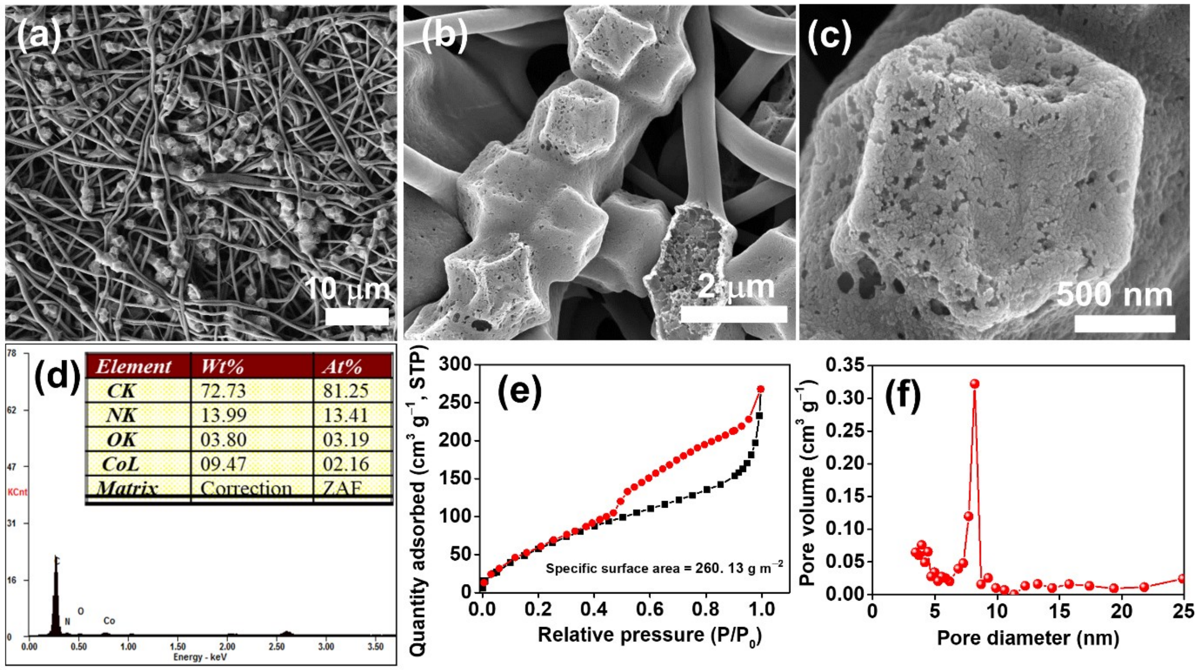

Fig. S7. (a-c) FE-SEM images of Co-N-CNFs (acid wash): (a) Low- and (b-c) high-magnification images**,** (d) EDS spectrum and the elemental composition (inset of d), (e) N_2 sorption isotherm and (f) BJH pore size distribution profiles.

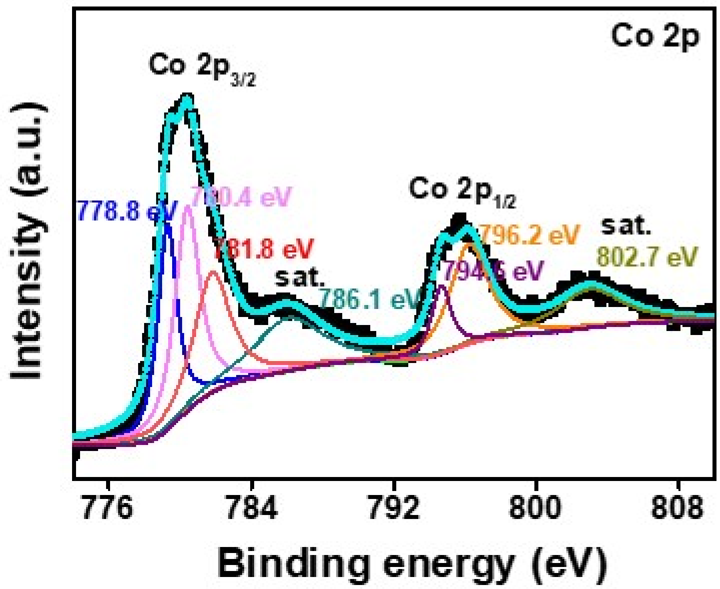

Fig. S8. Deconvoluted high-resolution XPS core-spectra of Co 2p for Co-N-CNFs electrode.

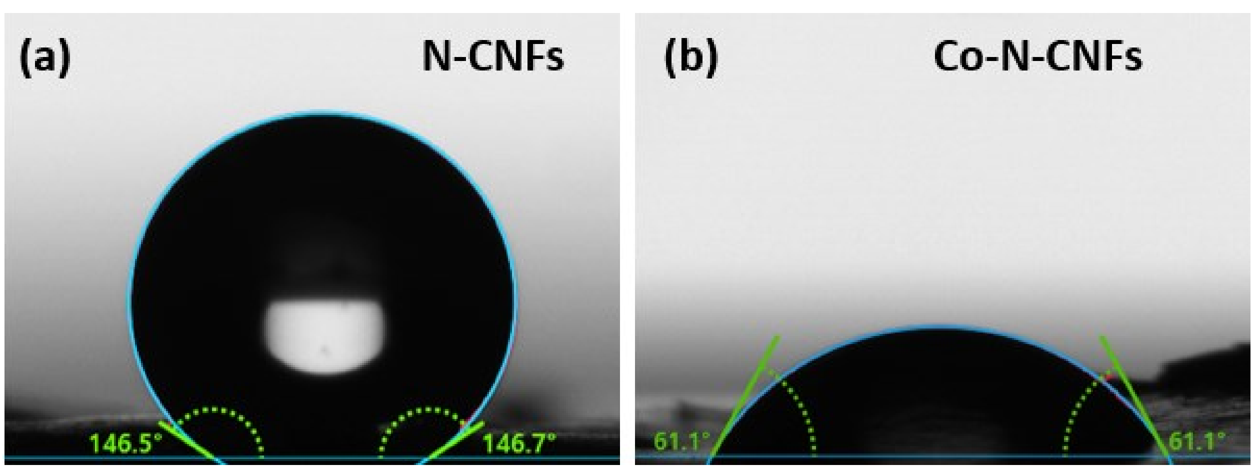

Fig. S9. Contact angle measurement of (a) pristine electrospun PAN nanofibers (EP-NFs) derived N-doped carbon nanofiber (N-CNFs) and (b) optimized electrospun PAN-ZIF-67-NFs derived Co-N-CNFs electrode.

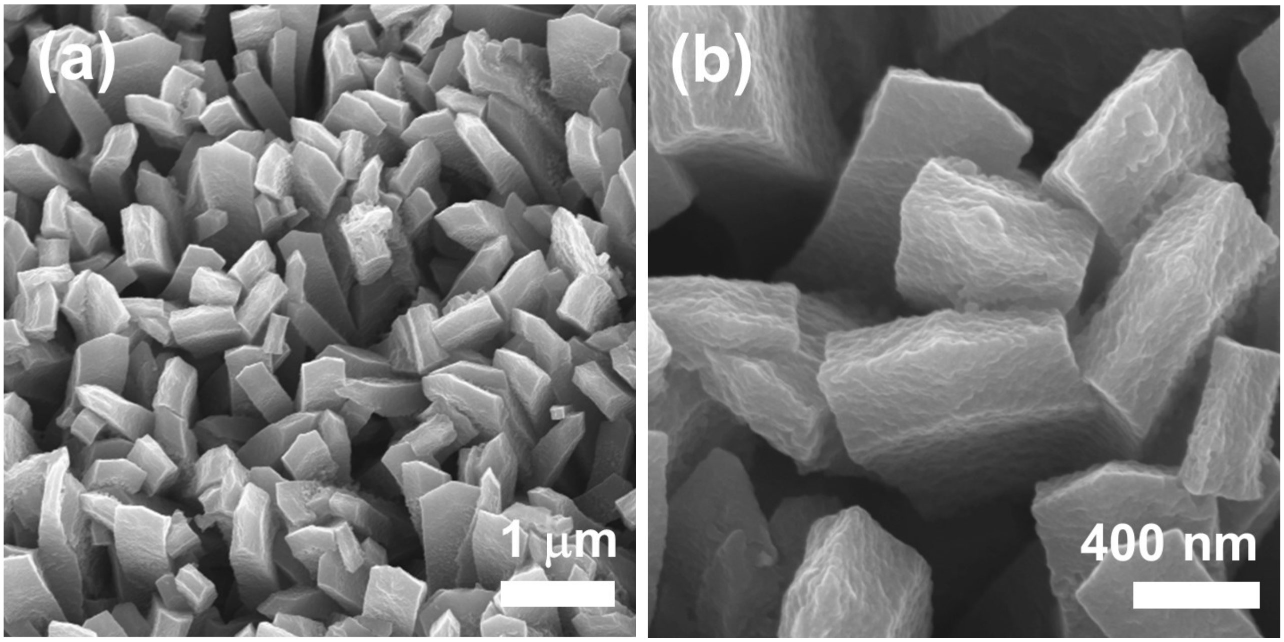

Fig. S10. (a and b) Low- and high-magnification FE-SEM images of Co-MOF/NF-derived Co_2P-N-C/NF micro-pillar array.

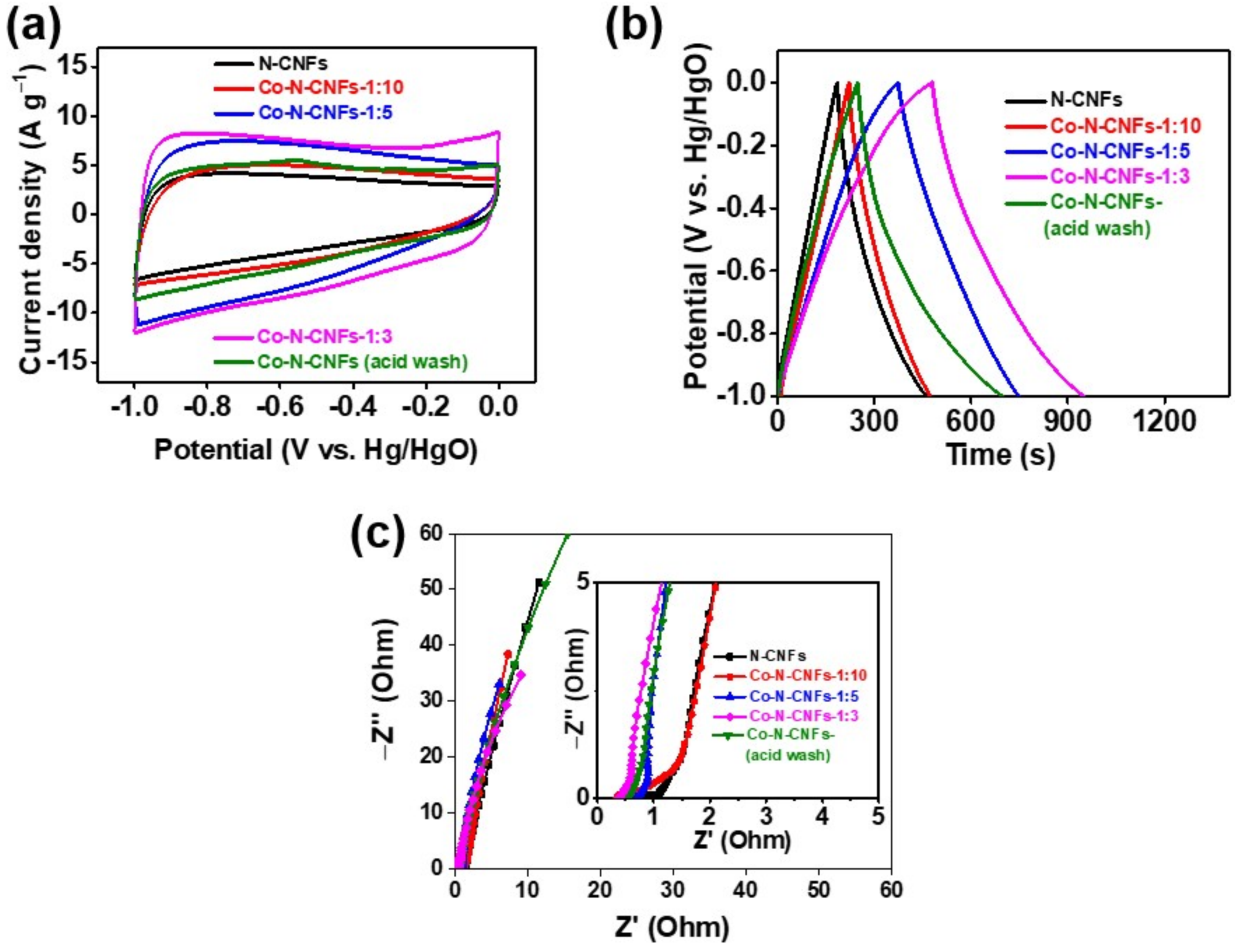

Fig. S11. (a) Cyclic voltammograms recorded at a fixed scan rate of 50 mV s^{-1}, (b) Galvanostatic charge-discharge (GCD) profiles at a fixed current density of 0.7 A g^{-1} and (c) EIS spectra at OCPs in the frequency range 0.01 – 10^5 Hz for N-CNFs and Co-N-CNFs of various composition (ZIF-67:PAN-1:10, 1:5, and 1:3) respectively.

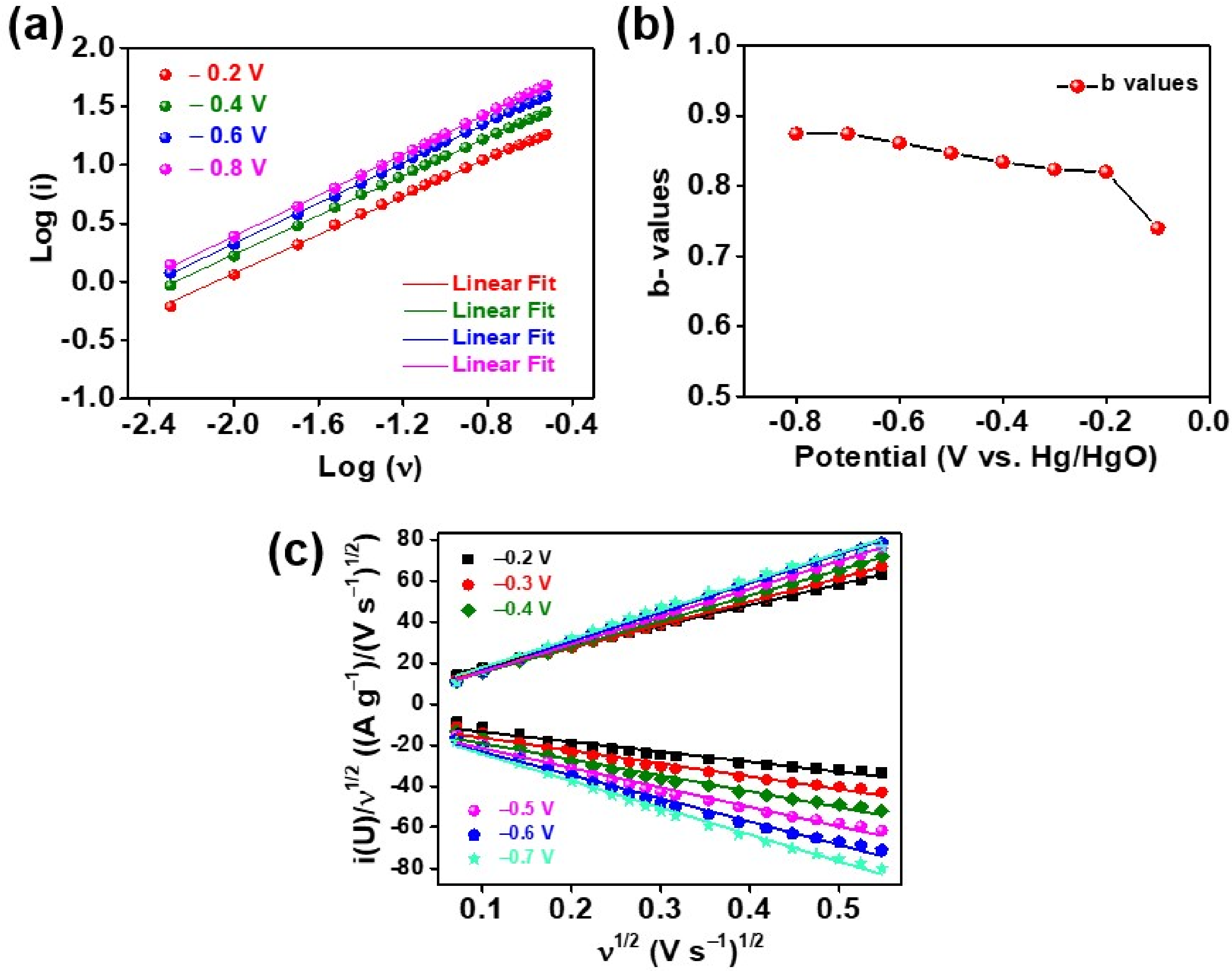

Fig. S12. (a) Plot between logarithmic current (log(i)) *vs.* logarithmic scan rates (log(υ)), (b) estimated "b-values" at various potentials, and (c) Plots of i(U)/$\upsilon^{1/2}$ versus $\upsilon^{1/2}$ (both in the anodic and cathodic regions at various potentials) and their respective linear fittings whose slopes and y-intercepts represents the values of k_1 and k_2 respectively.

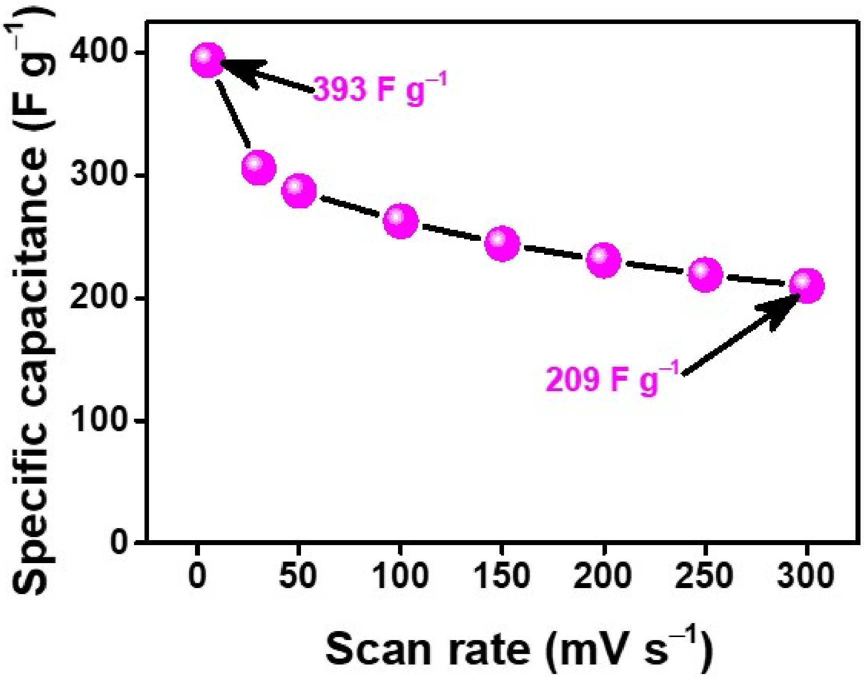

Fig. S13. Specific capacitance of Co-N-CNFs calculated from CV curves at various scan rates, from 5 mV s^{-1} to 300 mV s^{-1}.

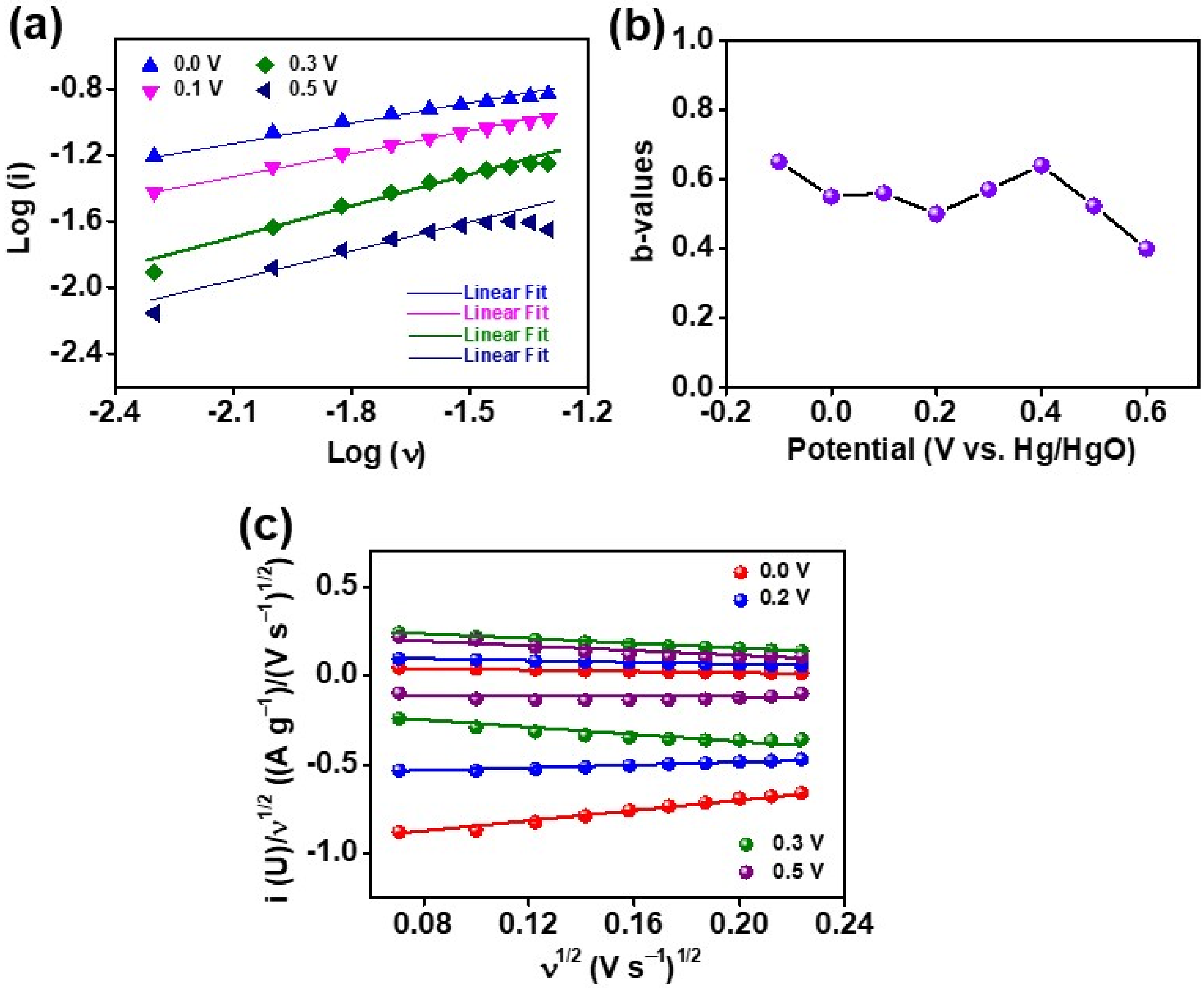

Fig. S14. (a) Plot between logarithmic current (log(i)) *vs.* logarithmic scan rates (log(υ)), (b) estimated "b-values" at various potentials, and (c) Plots of i(U)/$\upsilon^{1/2}$ versus $\upsilon^{1/2}$ (both in the anodic and cathodic regions at various potentials) and their respective linear fittings whose slopes and y-intercepts represents the values of k_1 and k_2 respectively.

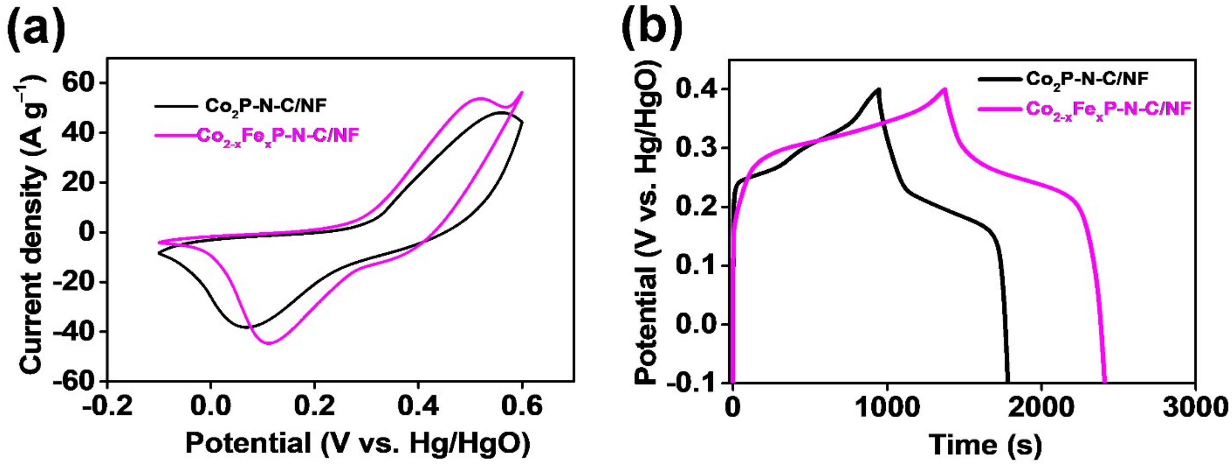

Fig. S15. Electrochemical analysis of Co-MOF/NF-derived Co_2P-N-C/NF electrode and CoFe-PBA/NF-derived $Co_{2-x}Fe_xP$-N-C/NF electrode (a) CV profiles recorded at 25 mV s^{-1} scan rate, and (b) GCD profiles recorded at 1 A g^{-1} current density.

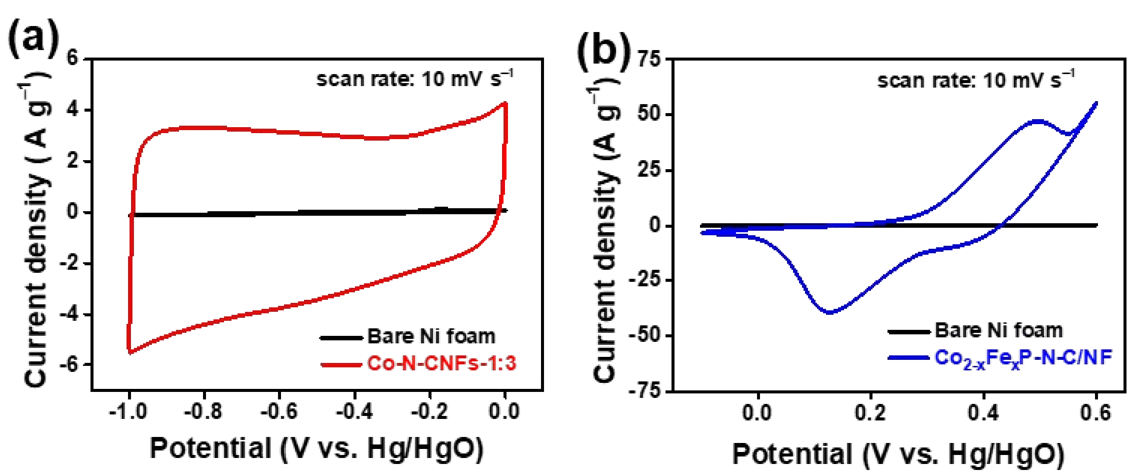

Fig. S16. CV profiles at the scan rate of 10 mV s^{-1} for bare Ni foam substrate in comparison to (a) Co-N-CNFs and (b) $Co_{2-x}Fe_xP$-N-C/NF electrode.

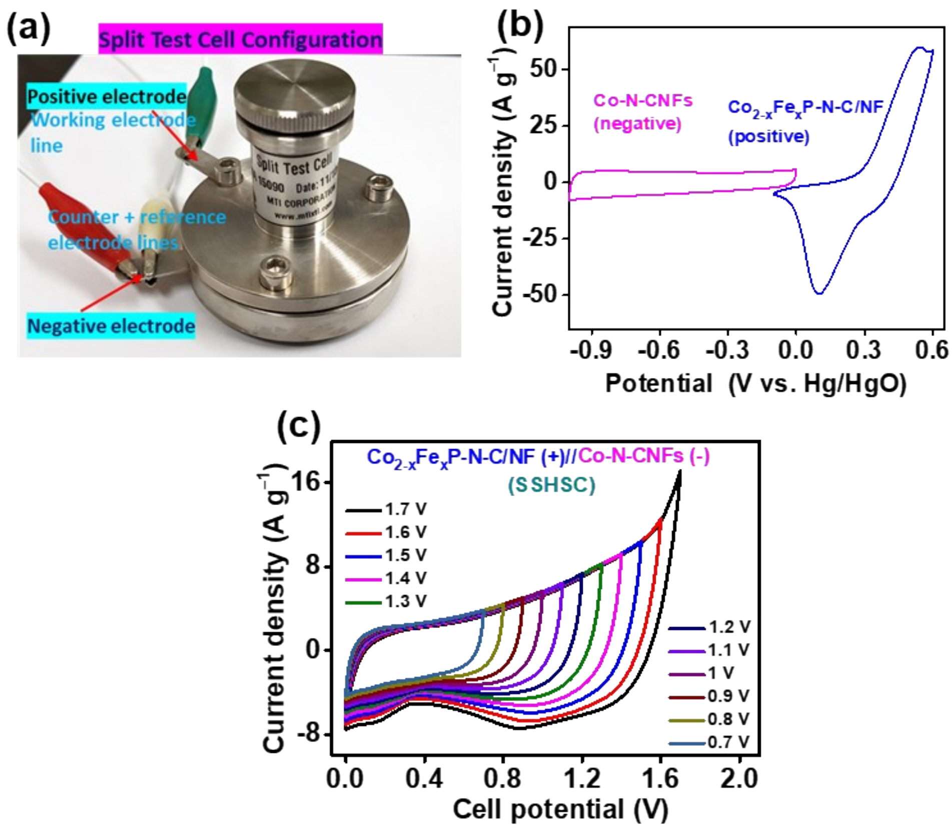

Fig. S17. a) Photographic image of hybrid supercapacitor fabricated using split test cell in which $Co_{2-x}Fe_xP$-N-C/NF positive and Co-N-CNFs negative electrodes are separated by a cellulose paper dipped in a PVA/KOH solid-gel electrolyte; (b) Combined half-cell CV profiles (scan rate: 20 mV s^{-1}) of Co-N-CNFs and $Co_{2-x}Fe_xP$-N-C/NF electrodes, and (c) CV profiles of the fabricated $Co_{2-x}Fe_xP$-N-C/NF (+)//Co-N-CNFs (–) solid state hybrid supercapacitor (SSHSC) device at a fixed scan rate of 50 mV s^{-1} showing the potential window extension upto 1.7 V respectively.

Table S1. Comparison of average sheet resistance between N-CNFs and Co-N-CNFs for ten measurements by four-point-probe surface resistivity meter.

Sample	**No. of measurement**	**Average Sheet resistance (Ω/sq.)**
N-CNFs	10	77.42
Co-N-CNFs	10	54.64

Table S2. The details of calculation of the specific capacitances at various current densities for the negative electrode (Co-N-CNFs) using equation (2), and corresponding to Fig. 5e-f.

Current (I) (mA)	**Mass (m) (mg)**	**Current density (I/m) (A g⁻¹)**	$\int U dt$ **(V s)**	$(\Delta U)^2$ **(V²)**	$C_{sc} = \frac{2I\int U dt}{m(\Delta U)^2}$ **(F g⁻¹)**
1	3	0.3	633.3	1	380
2		0.7	229.3		321
3		1	140		280
4		1.3	96.1		250
10		3.3	33.8		223
15		5	21.8		218
30		10	10.3		205
45		15	6.8		203
60		20	5		200

Table S3. The details of calculation of the specific capacities at various current densities for the $Co_{2-x}Fe_xP$-N-C/NF positive electrode using equation (4), and corresponding to Fig. 6d-e.

Current (I) (mA)	**Mass (m) (mg)**	**Current density (I/m) ($A\ g^{-1}$)**	$\int U dt$ (V s)	**Potential window (ΔU) (V)**	$C_s = \frac{2I\int U dt}{m\Delta U}$ ($mA\ h\ g^{-1}$)
2	2	1	310.50	0.5	345
3		1.5	205.20		342
4		2	151.65		337
5		2.5	120.24		334
6		3	99		330
8		4	72.45		322
10		5	55.98		311
20		10	24.57		273
30		15	14.70		245
40		20	9.94		221
50		25	7.56		210

Table S4. Electrochemical performance comparison of Co-N-CNFs electrode material with other recent negative electrode materials.

Electrode material	Electrolyte	Current density	Specific capacitance (F g^{-1})	GCD cycles@ current density	Capacitance retention [Coulombic efficiency]	References
Co-N-CNFs	6 M KOH	0.3 A g^{-1}; 1 A g^{-1}	380 ; 280	10,000 @10 A g^{-1}	97 % [99.8%]	**This work**
NPCF	1 M H_2SO_4	1 A g^{-1}	332	5,000 @1 A g^{-1}	98.9 % [NA]	1
NCF/graphene	6 M KOH	1 A g^{-1}	183	4,500 @1 A g^{-1}	92 % [NA]	2
Carbon-ZS	6 M KOH	0.1 A g^{-1}	285.8	1,000 @10 A g^{-1}	98.8% [NA]	3
N-doped OMC	1 M H_2SO_4	0.2 A g^{-1}	308	2,000 @ 2 A g^{-1}	- -	4
Nano porous carbon (NPC)	6 M KOH	2 mv s^{-1}	272	1,000 @ 8 A g^{-1}	- -	5
HPCNFs-N	2 M H_2SO_4	1 A g^{-1}	307.2	10,000 @5 A g^{-1}	98.2 % [NA]	6
Defect-enriched graphene block (DGB)	6 M KOH	1 A g^{-1}	235	10,000 @10 A g^{-1}	100% [NA]	7
HPNCs/CS	6 M KOH	1 A g^{-1}	280	- -	- -	8
3D-G/PANI	1 M H_2SO_4	1 A g^{-1}	777	60,000 @5 A g^{-1}	85 % [NA]	9
GQD embedded activated carbons (GEACS)	6 M KOH	1 A g^{-1}	388	10,000 @10 A g^{-1}	- -	10

Table S5. Electrochemical performance comparison of $Co_{2-x}Fe_xP$-N-C/NF electrode materials with other recent battery-type electrode materials.

Electrode material	Electrolyte	Current density ($A\ g^{-1}$/ $mA\ cm^{-2}$)	Specific capacity ($mA\ h\ g^{-1}$)	GCD cycles@ current density	Capacity retention [Coulombic efficiency]	References
$Co_{2-x}Fe_xP$-N-C/NF	6 M KOH	1 A g^{-1}	345 mA h g^{-1}	10,000 @ 20 A g^{-1}	86 % [99.5%]	**This work**
NiCoP@NF		1 A g^{-1}	2143 F g^{-1}	2,000 @ 10 A g^{-1}	73%	11
Zn-Ni-P NS	2 M KOH	2 mA cm^{-2}	384 mA h g^{-1}	10,000 @ 15 mA cm^{-2}	96 % -	12
Ni-MOF	3 M KOH	1 A g^{-1}	123 mA h g^{-1}	3000 @10 A g^{-1}	88.6%	13
Co(P,S)/CC	6 M KOH	1 A g^{-1}	295.8 mA h g^{-1}	10,000 @ 10 A g^{-1}	99%	14
Co_2P nanoflower	6 M KOH	1 A g^{-1}	416 F g^{-1}	- -	- -	15
Ni_2P	2 M KOH	1 A g^{-1}	843.25 F g^{-1}	1000@ 1 A g^{-1}	No obvious change	16
NiCoP	6 M KOH	1 A g^{-1}	571 C g^{-1}	3000@ 8 A g^{-1}	71.8%	17
Ni-P@$NiCo_2O_4$	6 M KOH+0.7 M LiOH	1 A g^{-1}	1240 F g^{-1}	- -	- -	18
Ni_2P@5%GR	3 M KOH	1 A g^{-1}	672.4 Fg^{-1}	2000@ 1 A g^{-1}	~29.74 % [~99%]	19
NiCoP nanoplates	1 M KOH	1 A g^{-1}	194 mA h g^{-1}	5000@ 10 A g^{-1}	81%	20

Table S6. Electrochemical performance comparison of our $Fe_xCo_{2-x}P$-N-C/NF (+)//Co-N-CNFs (−) SSHSC with other hybrid/asymmetric supercapacitors.

Device electrode materials (Positive//Negative)	Electrolyte	Current density (A g^{-1})	Specific capacity (mA h g^{-1})	Energy density@ power density	GCD cycles@ current density	Capacity retention [Coulombic efficiency]	Ref.
$Co_{2-x}Fe_xP$-N-C/NF//Co-N-CNFs	PVA/KOH	1 Ag^{-1}	104	84.72 W h Kg^{-1} @ 706 W k g^{-1}	10,000 @ 10 A g^{-1}	93 % [99.6 %]	**This work**
NiCoP/C//activated carbon	2 M KOH	1 Ag^{-1}	214.5 C g^{-1}	47.6 W h Kg^{-1} @798.9 W k g^{-1}	10,000 @ 10 A g^{-1}	78.1% -	21
Co_3O_4//carbon	6 KOH	2 Ag^{-1}	101 F g^{-1}	36 W h Kg^{-1} @1600 W k g^{-1}	2,000 @ 5 A g^{-1}	89% -	22
HPNCs/CS//HPNCs/CS	1 M Na_2SO_4	0.5 Ag^{-1}		16.2 W h kg^{-1} @ 0.45 k Wkg^{-1}	10,000@ 0.5 A g^{-1}	89 % [NA]	8
MOXC-700// Nano porous carbon (NPC)	6 KOH	0.5 Ag^{-1}	202.5	17.496 Wh kg^{-1} @ 388.8 W kg^{-1}	10,000@ A g^{-1}	>80% -	5
Co_2P nanoflowers//graphene	6 KOH	0.4 Ag^{-1}	76.8 F g^{-1}	8.8 Wh kg^{-1} @6 kW kg^{-1}	6000 @ 0.8 A g^{-1}	97% -	15
Ni_2P//Fe_2O_3	2 M KOH	0.5 Ag^{-1}	100 F g^{-1}	35.5 Wh kg^{-1} @400 W kg^{-1}	1000@10 mA cm^{-2}	96 % -	16
NiCoP//AC	6 M KOH	0.5Ag^{-1}	164 C g^{-1}	32Wh kg^{-1} @351W kg^{-1}	3000@	91.8% -	17
Ni-P@$NiCo_2O_4$//AC	6 M KOH and 0.7 M LiOH	1 Ag^{-1}	77	21Wh kg^{-1} @350W kg^{-1}	10,000@4 mA cm^{-2}	78.3% -	18
NiCoP nanoplates// graphene films	1 M KOH	2 A g^{-1}	43.8 mAh g^{-1}	32.9 Wh kg^{-1} @ 1301 W kg^{-1}	5000 @ 20 A g^{-1}	83% -	20
NSCGH//AC	2 M KOH		- -	21.1Whkg^{-1} @ 300 W kg^{-1}	10 000@	87.42% -	23
1T-$Mn_xMo_{1-x}S_{2-y}Se_y$// $MoFe_2S_4$–zSe_z	PVA/KOH	3 mA cm^{-2}	91 mA h g^{-1}	69 Wh kg^{-1}@ 0.985 kW kg^{-1}	10,000@ 50 mA cm^{-2}	83.5% -	24
$Ni_{3-x}Co_xS_4$//AC	6 M KOH	-	-	55.05 Wh kg^{-1} @14155.71 W k g^{-1}	5000@ 10 A g^{-1}	87.71% -	25
CoP/C//N-doped carbon shells	2 M KOH	1 A g^{-1}	59.3 F g^{-1}	16.14 Wh kg^{-1} @700 W kg^{-1}	5000 @ 7 A g^{-1}	99.5% -	26
3DPC/Co_3O_4//AC	3M KOH	1 A g^{-1}	60.76 F g^{-1}	21.1 Wh kg^{-1} @ 790 W kg^{-1}.	- -	- -	27
MoS_2/Ti_3C_2 //MoS_2/Ti_3C_2	PVA-H_2SO_4	2 mA cm^{-2}	347 mF cm^{-2}	17.4 µWh cm^{-2}@ 600 µW cm^{-2}	20 000@ 30 mA cm^{-2}	91.1%	28
$NiCo_2S_4$/NF// CNTs@Gr-CNF-5	6 M KOH	1 A g^{-1}	218 F g^{-1}	62.13 Wh kg^{-1} @ 789.66 W kg^{-1}	10,000 @ 1 A g^{-1}	94.98%	29

Reference:

1 C. Wang, C. Liu, J. Li, X. Sun, J. Shen, W. Han and L. Wang, *Chem. Commun.*, 2017, **53**, 1751–1754.

2 Q. Dong, G. Wang, H. Hu, J. Yang, B. Qian, Z. Ling and J. Qiu, *J. Power Sources*, 2013, **243**, 350–353.

3 S. Zhong, C. Zhan and D. Cao, *Carbon N. Y.*, 2015, **85**, 51–59.

4 Y. Song, L. Li, Y. Wang, C. Wang, Z. Guo and Y. Xia, *ChemPhysChem*, 2014, **15**, 2084–2093.

5 A. Mahmood, R. Zou, Q. Wang, W. Xia, H. Tabassum, B. Qiu and R. Zhao, *ACS Appl. Mater. Interfaces*, 2016, **8**, 2148–2157.

6 L.-F. Chen, Y. Lu, L. Yu and X. W. (David) Lou, *Energy Environ. Sci.*, 2017, **10**, 1777–1783.

7 Y. Dong, S. Zhang, X. Du, S. Hong, S. Zhao, Y. Chen, X. Chen and H. Song, *Adv. Funct. Mater.*, 2019, **29**, 1–10.

8 L. Xin, R. Chen, Q. Liu, J. Liu, Z. Li, R. Li and J. Wang, *New J. Chem.*, 2017, **41**, 12835–12842.

9 K. Li, J. Liu, Y. Huang, F. Bu and Y. Xu, *J. Mater. Chem. A*, 2017, **5**, 5466–5474.

10 Y. Qing, Y. Jiang, H. Lin, L. Wang, A. Liu, Y. Cao, R. Sheng, Y. Guo, C. Fan, S. Zhang, D. Jia and Z. Fan, *J. Mater. Chem. A*, 2019, **7**, 6021–6027.

11 Y. Lan, H. Zhao, Y. Zong, X. Li, Y. Sun, J. Feng, Y. Wang, X. Zheng and Y. Du, *Nanoscale*, 2018, **10**, 11775–11781.

12 T. T. Nguyen, J. Balamurugan, N. H. Kim and J. H. Lee, *J. Mater. Chem. A*, 2018, **6**, 8669–8681.

13 Y. Jiao, J. Pei, C. Yan, D. Chen, Y. Hu and G. Chen, *J. Mater. Chem. A*, 2016, **4**, 13344–13351.

14 A. M. Elshahawy, C. Guan, X. Li, H. Zhang, Y. Hu, H. Wu, S. J. Pennycook and J. Wang, *Nano Energy*, 2017, **39**, 162–171.

15 X. Chen, M. Cheng, D. Chen and R. Wang, *ACS Appl. Mater. Interfaces*, 2016, **8**, 3892–3900.

16 D. Wang, L.-B. Kong, M.-C. Liu, Y.-C. Luo and L. Kang, *Chem. - A Eur. J.*, 2015, **21**, 17897–17903.

17 Y. M. Hu, M. C. Liu, Y. X. Hu, Q. Q. Yang, L. Bin Kong and L. Kang, *Electrochim. Acta*, 2016, **215**, 114–125.

18 X. Li, R. Ding, L. Yi, W. Shi, Q. Xu and E. Liu, *Electrochim. Acta*, 2016, **222**, 1169–1175.

19 W. Du, S. Wei, K. Zhou, J. Guo, H. Pang and X. Qian, *Mater. Res. Bull.*, 2015, **61**, 333–339.

20 H. Liang, C. Xia, Q. Jiang, A. N. Gandi, U. Schwingenschlögl and H. N. Alshareef, *Nano Energy*, 2017, **35**, 331–340.

21 Q. Zhou, Y. Gong and K. Tao, *Electrochim. Acta*, 2019, **320**, 134582.

22 R. R. Salunkhe, J. Tang, Y. Kamachi, T. Nakato, J. H. Kim and Y. Yamauchi, *ACS Nano*, 2015, **9**, 6288–6296.

23 X. Yu, B. Lu and Z. Xu, *Adv. Mater.*, 2014, **26**, 1044–1051.

24 U. N. Pan, V. Sharma, T. Kshetri, T. I. Singh, D. R. Paudel, N. H. Kim and J. H. Lee, *Small*, 2020, **16**, 2001691.

25 M. Chuai, K. Zhang, X. Chen, Y. Tong, H. Zhang and M. Zhang, *Chem. Eng. J.*, 2020, **381**, 122682.

26 X. Zhang, S. Hou, Z. Ding, G. Zhu, H. Tang, Y. Hou, T. Lu and L. Pan, *J. Alloys Compd.*, 2020, **822**, 153578.

27 S. Li, K. Yang, P. Ye, K. Ma, Z. Zhang and Q. Huang, *Appl. Surf. Sci.*, 2020, **503**, 144090.

28 X. Wang, H. Li, H. Li, S. Lin, W. Ding, X. Zhu, Z. Sheng, H. Wang, X. Zhu and Y. Sun, *Adv. Funct. Mater.*, 2020, **30**, 0190302.

29 T. Kshetri, D. T. Tran, D. C. Nguyen, N. H. Kim, K. tak Lau and J. H. Lee, *Chem. Eng. J.*, 2020, **380**, 122543.